Received: 7 April 2022 | Revised: 27 June 2022 | Accepted: 28 June 2022

DOI: 10.1111/jace.18678

Journal of the American Ceramic Society

RESEARCH ARTICLE

$LnUO_4$-based glass–ceramic composites as waste forms for the immobilization of lanthanide-bearing uranium wastes

Kimbal T. Lu[1,2] | **Yingjie Zhang**[1] | **Tao Wei**[1] | **Gabriel L. Murphy**[3] | **Aurpa Bhuiyan**[1] | **Nicholas Scales**[1] | **Rongkun Zheng**[2]

[1]Australian Nuclear Science and Technology Organisation, Kirrawee DC, New South Wales, Australia

[2]School of Physics, The University of Sydney, Camperdown, New South Wales, Australia

[3]Nuclear Waste Management & Reactor Safety, Institute of Energy and Climate Research (IEK-6), Forschungszentrum Juelich (FZJ—Research Centre Julich), Julich, Germany

Correspondence
Yingjie Zhang, Australian Nuclear Science and Technology Organisation, Locked Bag 2001, Kirrawee DC, NSW 2232, Australia.
Email: yzx@ansto.gov.au

Funding information
German Federal Ministry of Education and Research (BMBF), Grant/Award Number: 02NUK060

Abstract

We report a comprehensive study on lanthanide monouranate–based glass–ceramic (GC) composites as potential waste forms for the immobilization of the lanthanide actinide fraction waste arising from the reprocessing of spent nuclear fuel (SNF). Although the crystalline $LnUO_4$ precursor prepared via a nitrate route can be well stabilized in a sodium aluminoborosilicate glass, the in situ crystallization of $EuUO_4$ in glass from oxide precursors (Eu_2O_3 and U_3O_8) is rather robust with regards to various processing conditions such as waste loadings, ceramic-to-glass ratios, and cooling rates. Scanning electron microscopy and transmission electron microscopy investigations revealed the detailed microstructures, where ~1–5-μm spheres for $NdUO_4$ and $EuUO_4$, and ~1–5-μm rectangular crystals for $DyUO_4$ and $HoUO_4$ were observed in residual glasses. As designed, the pentavalent uranium has been confirmed by diffuse reflectance spectroscopy. Overall, $LnUO_4$-based GC composite waste forms are chemically durable, offering flexible processing options with wide operating windows for SNF and process waste stream management.

KEYWORDS
glass–ceramics, nuclear waste, uranium/uranium compounds, waste disposal

1 | INTRODUCTION

Nuclear energy has attracted recent attention as an effective alternative to reduce carbon emissions.[1–5] However, the use of nuclear energy gives rise to the major issue of safe management of high-level radioactive wastes arising from the reprocessing of spent nuclear fuel (SNF).[6,7] Data published by the International Atomic Energy Agency indicated that over 370 kt of SNF were discharged from various nuclear reactors by 2013 globally.[8] Among them, one third was reprocessed and two thirds are in storage awaiting further conditioning and safe disposal.

The wastes generated from the reprocessing of SNF discharged from light water reactors contain a specific waste stream rich in both lanthanides as fission products and actinides, referred to as "rare earth/lanthanide actinide fraction (Ln–An fraction)."[9] Based on a rough estimation, 1 t of SNF discharged from light water reactors with a burn-up of 40–45 GW day contains ~15–25 kg of Ln–An fraction waste after storage for 5 years.[10] As such the

reprocessing of 700 t of SNF, the annual amount generated in Russia alone,[10] will produce ~10–17 tons of Ln–An fraction waste. Assuming a waste loading of ~20 wt% in an advanced waste form, the annual volume of waste form will be less than 20 m^3,[10] in comparison to that of borosilicate waste glass, for which the annual waste form volume is nearly a 100 times higher. This waste form volume reduction will require less repository space and therefore significantly reduce the cost for geological disposal. Uranium-rich radioactive wastes are also generated from the production of radiopharmaceuticals, such as ^{99}Mo[11] as well as uranium isotope enrichment, for example, the production of nuclear fuel (3.5–4.5-wt% ^{235}U) from natural uranium (0.7-wt% ^{235}U).[12] Note that the primary waste from uranium enrichment is a depleted uranium (DU) product, in which U_3O_8, UO_2, and UF_6 are the main DU forms in industry, with U_3O_8 being the most common and preferred state.[13]

All these U-rich radioactive wastes must be immobilized in highly durable materials as waste forms for final geological disposal. Owing to the low amount of uranium released from fluorite-structured UO_2 and brannerite (UTi_2O_6) under reducing environments, they have been primarily studied as potential host materials.[14–18] In addition, many durable titanate and phosphate mineral phases, such as zirconolite,[19–23] pyrochlore,[24–28] monazite,[29–32] xenotime,[32,33] and sodium zirconium phosphate (NZP),[34–36] have also been extensively investigated as potential waste forms. For high alpha-bearing wastes, such as plutonium residues, the incorporation of neutron absorbers (Gd and/or Hf) is often necessary to address the criticality concerns.[37]

Metal monouranates, MUO_4, have attracted recent interest due to their implications in the nuclear industry, for example, their association with UO_2-based nuclear fuels such as accident tolerant fuels and their potential role in SNF management.[38,39] As such, some metal monouranates have been investigated specifically on phase formation, structures and microstructures, and spectroscopies.[40–42] It is well established that cubic-structured phases are dominant in the UO_2–Ln_2O_3 system for the entire compositional range.[43,44] Given Ln–An-fraction waste contains mainly Ln and U, the waste form design strategy considers $LnUO_4$ or related durable mineral phases. As large amounts of Ln are expected as the transmutation products in the SNF in storage, the chemical stability also needs to be considered in the design of suitable waste forms, such as $LnUO_4$.[45] As most of the U-rich waste also contains some processing chemicals and impurities that are not readily being incorporated in the designed ceramic phases,[46] the chemical flexibility of the waste form design must also be taken into consideration, in addition to the durable phase for An, in order to accommodate these processing chemicals and impurities. As such, glass–ceramics (GCs) as composite waste forms have emerged as the focus of recent studies.[47–50] The primary advantages of GCs or glass crystalline material[51,52] over conventional full ceramics or glasses are the combined chemical flexibility of glass, which allows for the accommodation of processing chemicals and impurities, with the high chemical durability of ceramic phases to host Ln and An ions within the crystal structures.[52] Additionally, the addition of glass in GCs acts as a double barrier to contain the ceramic phases with An and also offers advantage in ease of processing as no milling step is required.[52]

Despite recent advances on various candidate waste forms for SNF management, many technical challenges exist, which must be addressed. More robust and flexible waste forms are yet to be developed. The primary goal of the current work was to investigate the feasibility of $LnUO_4$-based GC composites as advanced waste forms for the immobilization of U-rich radioactive waste streams containing processing chemicals and impurities, including the Ln–An fraction waste from reprocessing of SNF discharged from light water reactors. Herein, we report the first comprehensive study on the development of $LnUO_4$–GC composite waste forms, including the stabilization and crystallization of $LnUO_4$ in glass, structures and microstructures, processing conditions, and chemical durability of the fabricated GC waste forms. Overall, the $LnUO_4$-based GC system is robust allowing for very flexible processing conditions, and the waste forms fabricated via in situ crystallization from mixed oxides show good chemical durability.

2 | EXPERIMENTAL PROCEDURES

2.1 | Synthesis

Sodium carbonate (99.9%), aluminum oxide (99.5%+), boric acid (99.5%+), silicon dioxide (99.9%+), neodymium/europium/dysprosium/holmium (Nd/Eu/Dy/Ho) nitrate hexahydrate, Nd_2O_3, and Eu_2O_3 were purchased from Sigma-Aldrich. Sodium carbonate was pre-dried in an oven at 300°C for 3 h and other solid reagents were pre-dried at 100°C for 3 h prior to use. The glass precursor with a stoichiometry of $Na_2AlBSi_6O_{16}$ was prepared by mixing calculated amounts of Na_2CO_3, Al_2O_3, H_3BO_3, and SiO_2 with the required molar ratios and then calcined in air at 600°C for 4 h. The calculated oxide compositions were Na_2O (12.19 wt%), Al_2O_3 (10.03 wt%), B_2O_3 (6.85 wt%), and SiO_2 (70.93 wt%).

As previously stated, the waste form design strategy considers the investigation of $LnUO_4$–GC composites as

potential waste forms, given the Ln–An-fraction waste contains Ln and U as the main chemical elements. It is essential to understand whether a wide range of Ln ions can be stabilized as crystalline $LnUO_4$ in glass. Subsequently, the in situ crystallization of $LnUO_4$ in glass from mixed oxide precursors must be investigated under various processing conditions such as ceramic to glass ratios and cooling rates. The latter is a critical aspect of the feasibility studies in regard to waste form processing as a majority of the waste streams will be dried and calcined as mixed oxides. In order to address the previous two aspects, the $LnUO_4$–GC samples were synthesized with the glass precursor via two processing routes: (1) nitrate route with $LnUO_4$ precursor prepared using Ln and uranyl nitrates; (2) oxide route with in situ formation of $LnUO_4$ in glass from Ln_2O_3 and U_3O_8.

For nitrate route, uranyl nitrate and $Ln(NO_3)_3$ in equal molar ratio were dissolved in a beaker with deionized water. The solution was dried in an oven at 100°C. The dried mixture was calcined at 750°C for 6 h. The obtained $LnUO_4$ precursors were mixed and ground with different amounts of glass precursor using an agate mortar and pestle, pelletized under a pressure of 100 MPa, and then sintered at 1200°C in air for 6 h in a tube furnace with heating and cooling rate of 5°C min^{-1}.

For oxide route, U_3O_8 and Ln_2O_3 in equal molar ratios were mixed with required amounts of glass precursor. The mixtures were ground in an agate mortar and pestle, pelletized under a pressure of 100 MPa, and then sintered at 1200°C in air for 6 h with various cooling rates: 1, 5, and 10°C min^{-1}. The detailed synthesis parameters for all GC samples are summarized in Table 1.

Earlier works on pyrochlore GCs with the same glass composition confirmed that sintering temperatures at above 1100°C for over 3 h are necessary to make well-crystallized GC composites.[53,54] As such, the optimized sintering condition (1200°C for 6 h) for pyrochlore GC composites was chosen to prepare all the samples in this study. In general, homogeneous mixing of all chemical mixtures is desirable to produce uniform ceramics and GC composites. As such, ball-mill is commonly used especially for the preparation of pure ceramics. However, one of the advantages of GCs is the minimal requirement for milling in the presence of a glass. Consequently, the gentle grinding of the mixture is sufficient to produce uniform GCs composites.

2.2 | Characterization

Powder X-ray diffraction (XRD) patterns were acquired using a Bruker D8 X-ray diffractometer using Cu K_α radiation in an angular range of 5–120 2θ with a step size of 0.02°2θ and an acquisition time of 2 s per step. A Zeiss Ultra Plus scanning electron microscope (SEM), Carl Zeiss NTS GmbH, Oberkochen, Germany, operating at 15 kV, equipped with an Oxford Instruments X-Max 80-mm^2 silicon drift detector (SDD) X-ray microanalysis system was used to examine microstructures, and energy-dispersive X-ray spectroscopy (EDS) was calibrated with a Cu standard for elemental analysis. Solid samples were embedded in resin, polished to a 1-μm finish, and carbon-coated for SEM. Transmission electron microscopy (TEM) analysis was carried out using a JEOL 2200FS (JEOL Ltd, Japan)

TABLE 1 $LnUO_4$ glass–ceramic (GC) samples fabricated at 1200°C for 6 h in air via both nitrate and oxide routes with various processing conditions

Sample ID	$LnUO_4$[a] (wt%)	U_3O_8 and Ln_2O_3 (wt%)	Glass (wt%)	Cooling rate (°C min^{-1})
Nd1	50.0	–	50.0	5.0
Eu1	50.0	–	50.0	5.0
Dy1	50.0	–	50.0	5.0
Ho1	50.0	–	50.0	5.0
Eu2	–	80.0	20.0	5.0
Eu3	–	70.0	30.0	5.0
Eu4	–	60.0	40.0	5.0
Eu5	–	50.0	50.0	5.0
Eu6	–	50.0	50.0	1.0
Eu7	–	50.0	50.0	10.0
Nd2	–	50.0	50.0	5.0
Ho2	–	50.0	50.0	5.0

[a]Precursors prepared via nitrate route.

operated at 200 kV, fitted with an Oxford X-Max SDD for EDS. Specimens consist of crushed grains dispersed in ethanol and then dispensed onto a holey carbon film supported on a TEM copper mesh grid. Diffuse reflectance spectra (DRS) were measured in the UV–Vis and NIR regions on an Agilent Cary 5000 spectrophotometer with a Labsphere Biconical Accessory. PCT leaching experiments (ASTM C1285) at 90°C were carried out in aqueous media by prescribed protocols.[55] The leachates were filtered, acidified, and analyzed after 7 days of leaching using an Agilent 7700× inductively coupled plasma–mass spectrometry.

3 | RESULTS AND DISCUSSION

3.1 | Synthesis

Previous research[43,44] confirmed that Ln_2O_3 can react with UO_2 under reducing conditions to form stable solid solutions with cubic fluorite structures. More recently, $DyUO_4$ and $HoUO_4$ were synthesized by sintering in argon at 1400°C.[56] It is evident that pentavalent U in $LnUO_4$ phases can be stabilized by sintering in argon with the addition of trivalent Ln due to the chemical control for charge neutrality. However, the low oxygen fugacity in melting glass allows the formation of $LnUO_4$ in glass by sintering in air. As such all $LnUO_4$–GC samples were synthesized by sintering in air. The primary goal is to determine whether a wide range of crystalline $LnUO_4$ can be stabilized in glass. Subsequently, it is important to investigate the in situ crystallization of $LnUO_4$ in glass and the processing parameters with regard to ceramic-to-glass ratios and cooling rates.

3.2 | Structures and microstructures

The XRD patterns of the four $LnUO_4$–GC (Nd1, Eu1, Dy1, and Ho1) samples are shown in Figure 1. The similar XRD patterns suggest that pure crystalline $LnUO_4$ was produced, corresponding to the designed phases in cubic fluorite structures with space group $Fm\bar{3}m$. The slight peak shifts to higher angles among the samples are attributed to the cell parameter and volume reductions owing to the lanthanide contraction from Nd to Ho, with ionic radii in eightfold coordination environment ranging from 0.1109 (Nd^{3+}), 0.1066 (Eu^{3+}), 0.1027 (Dy^{3+}) to 0.1015 (Ho^{3+}) nm.[57] Subsequently, the cell parameters were refined using X'pert Highscore Plus and summarized in Table 2. The refined cell parameters for both $DyUO_4$ and $HoUO_4$ are close to the values previously reported.[56] Note, pure amorphous glass with this composition gives no obvious XRD features except a few weak humps at around 5°, 23°, 42°, and 61° (2θ).[53] In the case of GCs with light crystalline phases, these humps are visible in the XRD patterns. However, with crystalline phases containing heavy U and Ln elements in this work, the contribution from the amorphous glass has essentially become the background level.

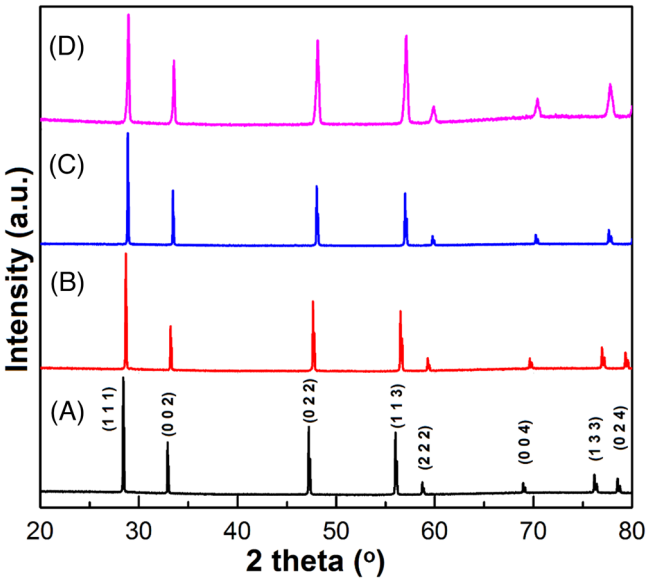

FIGURE 1 X-ray diffraction patterns of Nd1 (A), Eu1 (B), Dy1 (C), and Ho1 (D) showing $LnUO_4$ as the crystalline structures

TABLE 2 Cell parameters refinements for Nd1, Eu1, Dy1, and Ho1 from X-ray diffraction (XRD) data using X'pert Highscore Plus

Sample ID	Ionic radius (nm)	Parameter *a* (nm)	Cell vol. (nm^3)
Nd1	0.1109	0.54459	0.1615
Eu1	0.1066	0.54002	0.1575
Dy1	0.1027	0.53573	0.1537
Ho1	0.1015	0.53532	0.1534

The backscattered SEM images of Nd1 (Figure 2A,B), Eu1 (Figure 2C,D), Dy1 (Figure 3A,B), and Ho1 (Figure 3C,D) displayed $LnUO_4$ phases (bright) crystallized in the residual glass (dark). The $LnUO_4$ grains are considerably small (1–5 μm), which are desirable, with an average grain size of ~3 μm. The small grains tend to agglomerate and form clusters. Although the $NdUO_4$ and $EuUO_4$ crystallites exhibited typical spherical shapes (Figure 2), the $DyUO_4$ and $HoUO_4$ crystallites generally exhibited rectangular structures (Figure 3). Multiple-point EDS analyses confirmed that all four samples display the equal U:Ln atomic ratio as designed (Figures S1–S4). The U and Ln are dominantly in $LnUO_4$ with the U/Ln partitioning factors of 6–12 between $LnUO_4$ phases and residual glasses. Overall, $LnUO_4$–GC samples fabricated

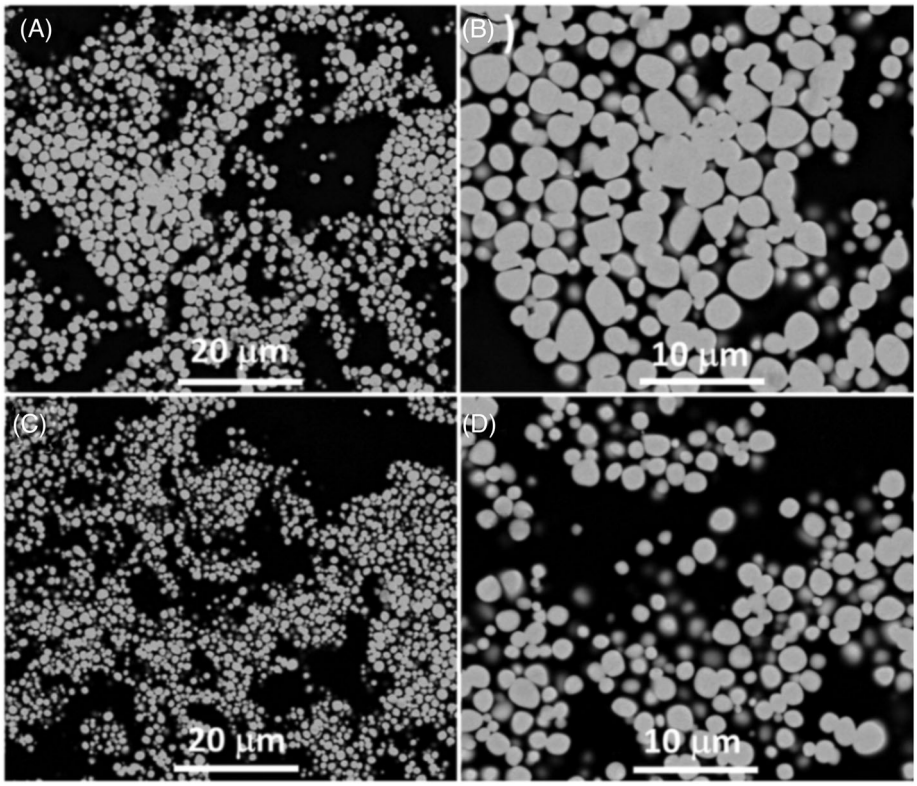

FIGURE 2 Backscattered scanning electron microscopy (SEM) images of Nd1 (A and B) and Eu1 (C and D) showing $NdUO_4$ in Nd1 and $NdUO_4$ in Eu1 as the crystalline phases

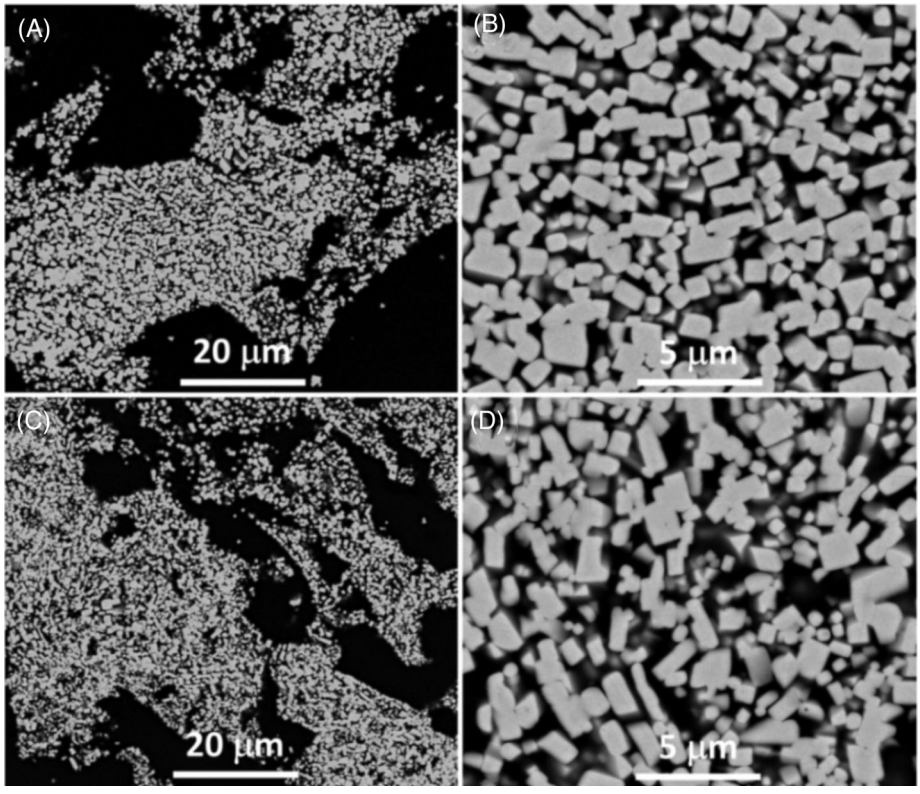

FIGURE 3 Backscattered scanning electron microscopy (SEM) images of Dy1 (A and B) and Ho1 (C and D) showing $DyUO_4$ in Dy1 and $HoUO_4$ in Ho1 as the crystalline phases

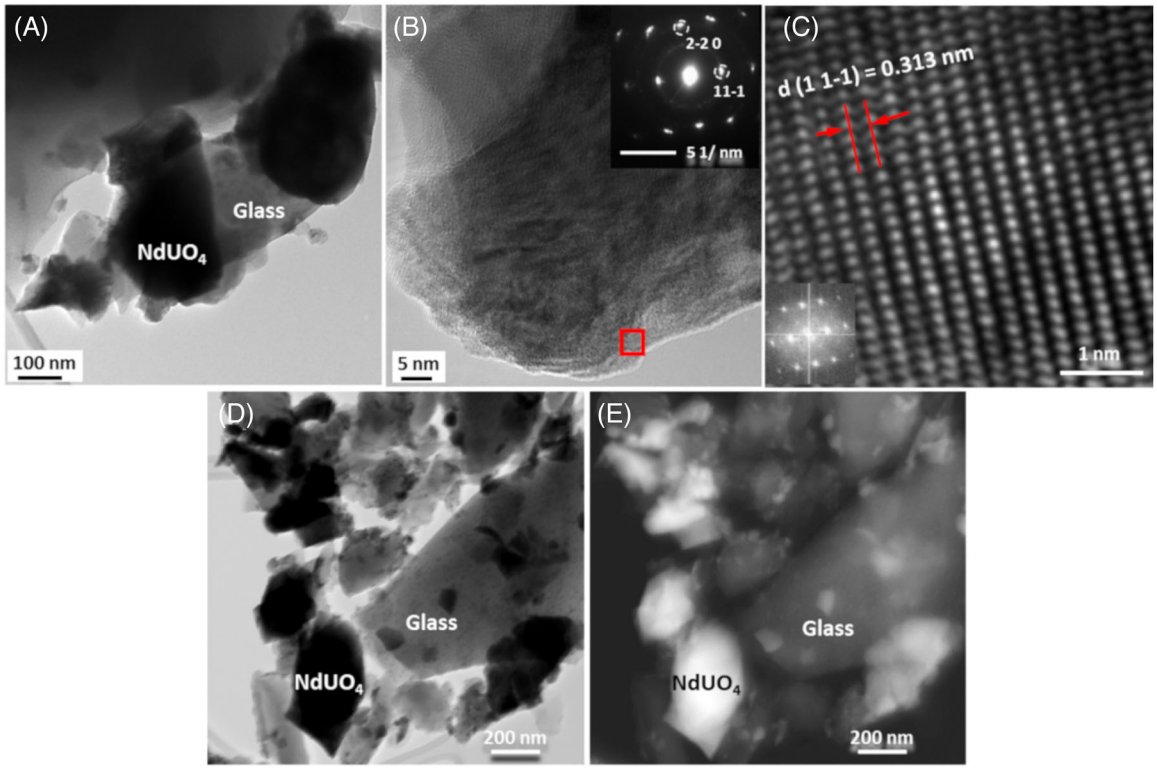

FIGURE 4 Transmission electron microscopy (TEM) of Nd1: a TEM image showing $NdUO_4$ and glass (A); a high magnification image from an $NdUO_4$ grain with an inserted selected area electron diffraction (SAED) pattern in [1 1 2] zone axis (B); an high-resolution transmission electron microscopy (HRTEM) image from a position marked in (B) with an inserted fast Fourier transform (FFT) image in [1 1 2] zone axis (C); STEM bright field (D) and the corresponding dark field (E) images showing $NdUO_4$ grains and glass

using premade $LnUO_4$ precursors confirmed that $LnUO_4$ can be stabilized in glass with only minor dissolution after heat treatment at 1200°C in air.

Both of the samples Nd1 and Dy1 were further investigated by TEM. For Nd1, a bright field TEM image (Figure 4A) displayed $NdUO_4$ grains in the residual glass. A high magnification image of an $NdUO_4$ grain with an inserted selected area electron diffraction (SAED) pattern in the [1 1 2] zone axis is shown in Figure 4B, which was indexed to the $NdUO_4$ with a cubic fluorite structure. A high-resolution TEM (HRTEM) image in the [1 1 2] zone axis (Figure 4C) showed fluorite lattice fringes with a fast Fourier transform (FFT) image in the inset and a measured d (1 1 1) spacing value of 0.313 nm, consistent with the crystal structure data (a = 0.54459 nm in Table 2). A bright STEM image (Figure 4D) and the corresponding dark STEM image (Figure 4E) unveiled $NdUO_4$ grains adjacent to the residual glass.

For Dy1, a bright field STEM image (Figure 5A) showed $DyUO_4$ grains in dark contrast and surrounding residual glass in gray contrast, and the corresponding dark field image was shown in Figure 5B. An SAED pattern of a $DyUO_4$ grain in the [0 0 1] zone axis (Figure 5C) was indexed to fluorite crystal structure. An HRTEM image in the [1 1 −2] zone axis showed lattice fringes with an FFT image and indexed SAED pattern as insets (Figure 5D) and a measured d (1 1 1) spacing value of 0.312 nm, which corresponds closely to the d (1 1 1) spacing value of the full ceramic $DyUO_4$ (0.310 nm).[56]

3.3 | Uranium valence

It is essential to understand the exact U valences in the designed waste forms as the U valences play an important role in controlling U releases to the environment.[58] Several spectroscopic techniques, such as X-ray photoelectron spectroscopy, X-ray absorption near-edge spectra, and DRS, have been widely used to probe U valences in mixed oxides.[59–64] In general, uranium can be stabilized in 4+ ($5f^2$ electron configuration), 5+ ($5f^1$), or 6+ ($5f^0$) valence states in oxides depending on the processing redox conditions and the possible presence of other low valence cations for charge compensation.[60] In DRS, although the U^{4+} ion gives sharp zero-phonon line and broad vibronic absorptions from the visible to infrared spectral range, the U^{5+} ion is solely confined to the near infrared as it derives only from the crystal-field splitting

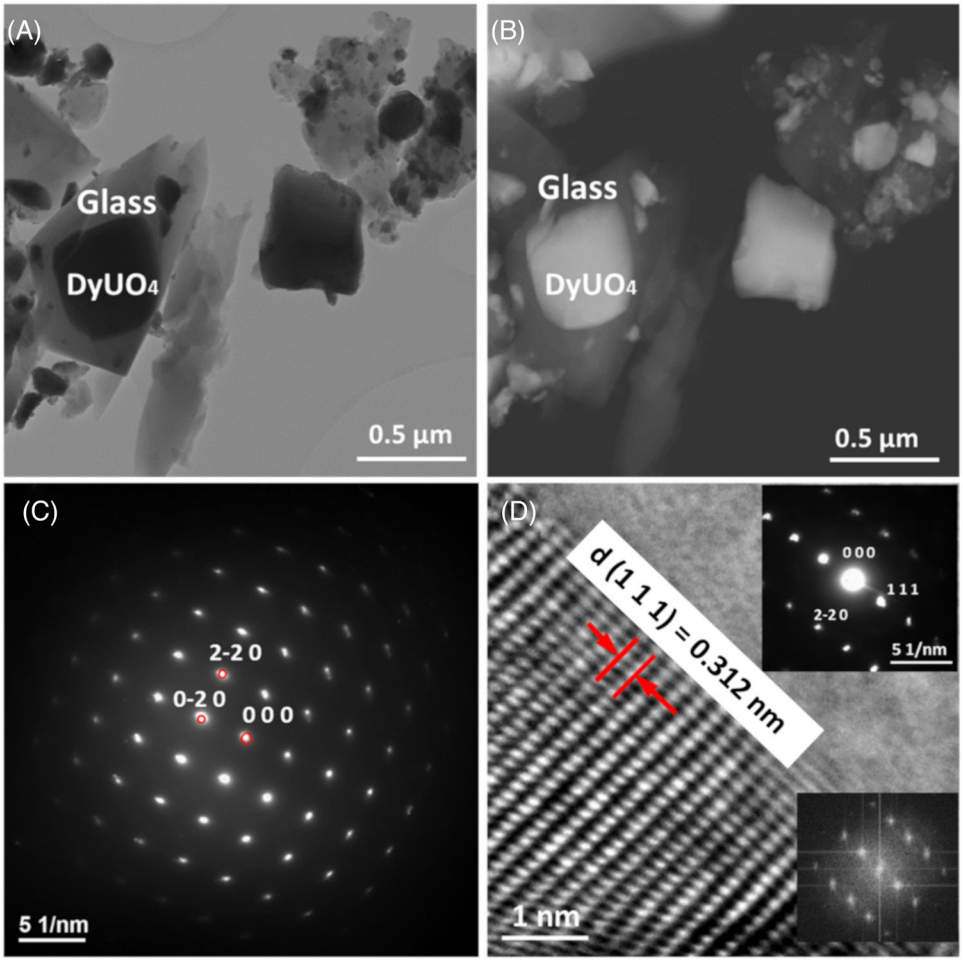

FIGURE 5 Transmission electron microscopy (TEM) of Dy1: high-resolution transmission electron microscopy (STEM) bright field (A) and the corresponding dark field (B) images showing $DyUO_4$ grains and surrounding glass; a selected area electron diffraction (SAED) pattern of a $DyUO_4$ grain in [0 0 1] zone axis (C) and an high-resolution transmission electron microscopy (HRTEM) image in [11−2] zone axis from the edge of a $DyUO_4$ grain with inserted SAED pattern and fast Fourier transform (FFT) image (D)

of $^2F_{5/2}$–$^2F_{7/2}$ components (split by spin-orbit coupling) of the ^2F electronic state,[62–64] with the sharp electronic transitions observable from the splitting of $^2F_{7/2}$ at 1538–833 nm (6500–12 000 cm^{-1}) range depending on the local ion coordination environment.[62–64] In contrast, only broad charge-transfer bands in the blue and near-ultraviolet spectral regions are characteristic for the U^{6+} ion with no f-electrons.

DRS was successfully used to confirm the pentavalent U ions in $DyUO_4$ and $HoUO_4$ compounds sintered in argon.[56] Similarly, it can provide useful information on U valences in $LnUO_4$–GC samples. The DR spectra in the near-infrared region (850–2500 nm) for samples Nd1, Eu1, Dy1, and Ho1 are shown in Figure 6 with the area (1400–1800 nm) highlighted. It is apparent that all DR spectra showed a small absorption band at around 900 nm and a major absorption band at ~1615 nm, confirming the U^{5+} ion on the eightfold coordinated environment, consistent with the cubic fluorite structures. These findings are also consistent with the earlier study of $DyUO_4$ and $HoUO_4$ compounds with absorption bands at ~1615 nm, corresponding to the U^{5+} ion in an eightfold coordination environment[54] as the absorption band for the U^{5+} ion in an octahedral coordination environment would be shifted to lower wavelength at around 1585 nm.[56,64]

3.4 | Effect of $EuUO_4$-to-glass ratio or waste loading

To examine the effect of ceramic-to-glass ratios on the phase formation in glass, a set of four $EuUO_4$–GC samples (Eu2–Eu5) with designed $EuUO_4$-to-glass ratios of 50%, 60%, 70%, and 80% were fabricated via an oxide route and heat treated at 1200°C (Table 1). The XRD results (Figure 7) confirmed that $EuUO_4$ in the cubic fluorite structure is the only crystalline phase across the four samples, suggesting a robust system with regard

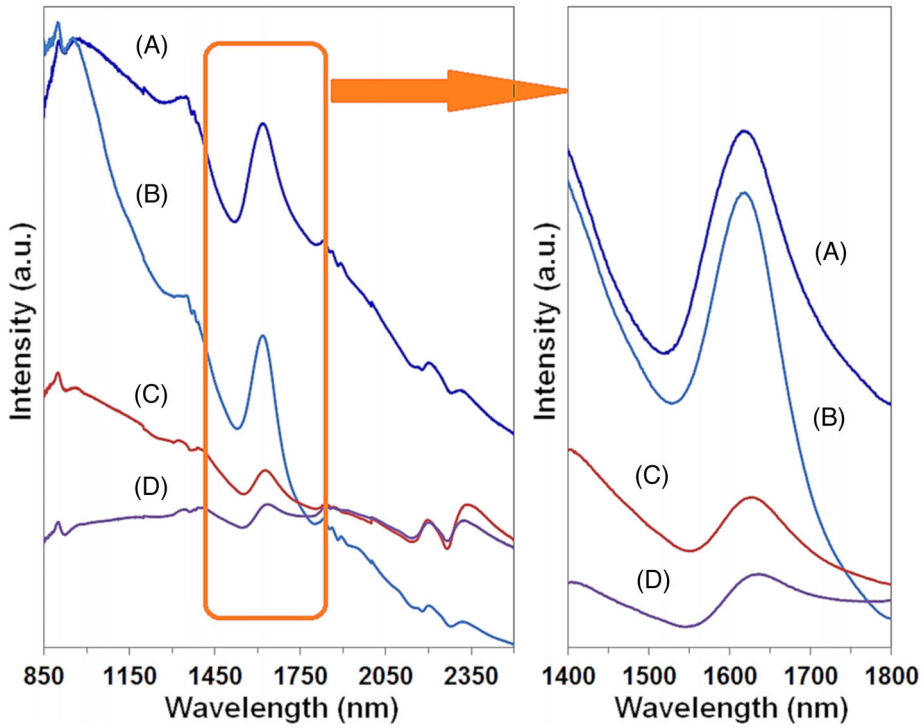

FIGURE 6 Diffuse reflectance spectra in the NIR region (850–2500 nm) of Nd1 (A), Eu1 (B), Dy1 (C), and Ho1 (D), with the expansion of the 1400–1800-nm region on the right-hand side

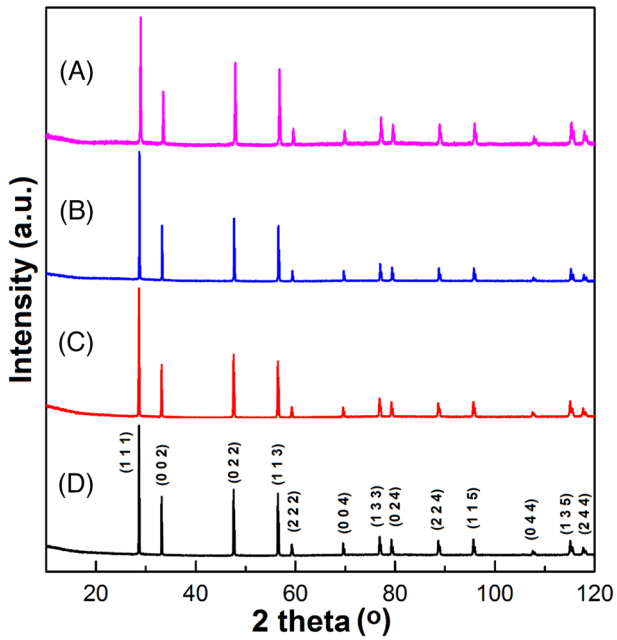

FIGURE 7 Effect of $EuUO_4$-to-glass ratio: Eu2, 50 wt% (A), Eu3, 60 wt% (B), Eu4, 70 wt% (C), and Eu5, 80 wt% (D) showing $EuUO_4$ as the only crystalline phase

to waste loadings. Backscattered SEM images (Figure 8) showed similar microstructures with round $EuUO_4$ crystallites distributed in residual glasses. The average grain sizes remained consistent when the $EuUO_4$-to-glass ratios were increased from 50% to 60%, and the average grain sizes increased gradually when the $EuUO_4$-to-glass ratios were ≥70%. It is also notable that some grains started to agglomerate at higher $EuUO_4$-to-glass ratios for Eu4 and Eu5 (Figure 8C,D) showing increasing amounts of clustered $EuUO_4$ crystallites in residual glasses. The tendency of crystallites to form clusters is largely due to the shorter distances between the nucleated $EuUO_4$ grains as a result of increasing the $EuUO_4$-to-glass ratio. EDS analyses confirmed equal Eu:U atomic ratio in $EuUO_4$ crystallites (Figures S5 and S6). No obvious higher $EuUO_4$ dissolution in glass was observed with higher waste loadings (Figures S5 and S6).

3.5 | Effect of cooling rate

The effect of cooling rate on the phase formation and microstructures was further studied using a set of three $EuUO_4$–GC samples (Eu6, Eu5, and Eu7) with a fixed equal ceramic-to-glass ratio (50 wt%:50 wt%, see Table 1). The cooling rate of 1, 5, and 10°C/min were applied to the samples after heat treatment at 1200°C for 6 h in air. The XRD results (Figure 9) showed essentially the same patterns for $EuUO_4$ in the cubic fluorite structure, suggesting a wide processing window with regards to the cooling rate. This is quite important for industrial processing of waste forms, as wider processing parameters, such as

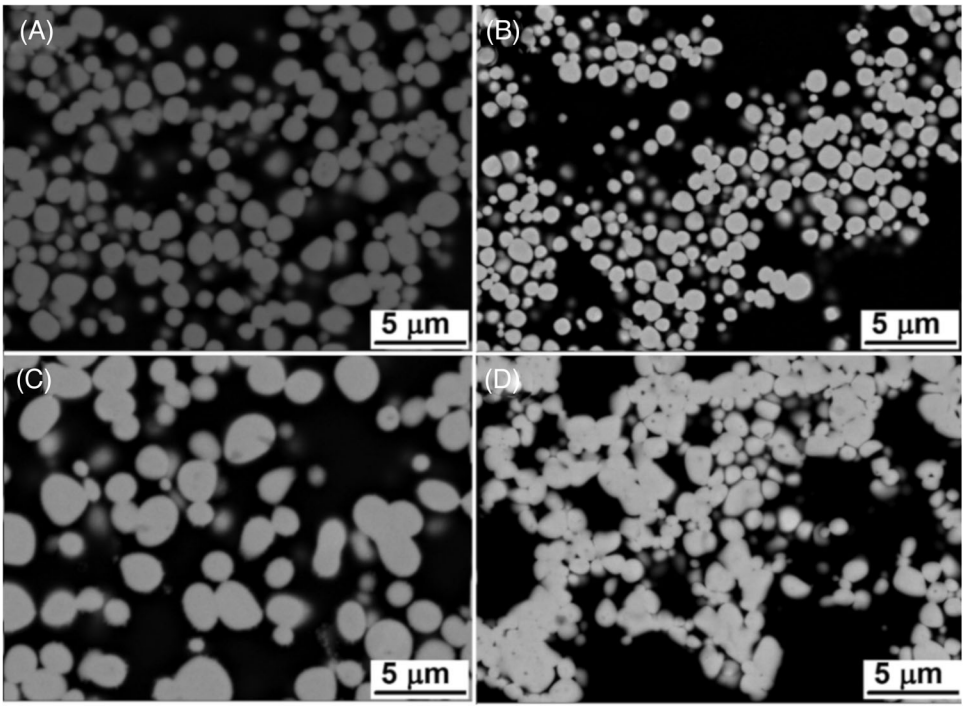

FIGURE 8 Backscattered scanning electron microscopy (SEM) images of Eu2, 50 wt% (A), Eu3, 60 wt% (B), Eu4, 70 wt% (C), and Eu5, 80 wt% (D) showing $EuUO_4$ as the only crystalline phase

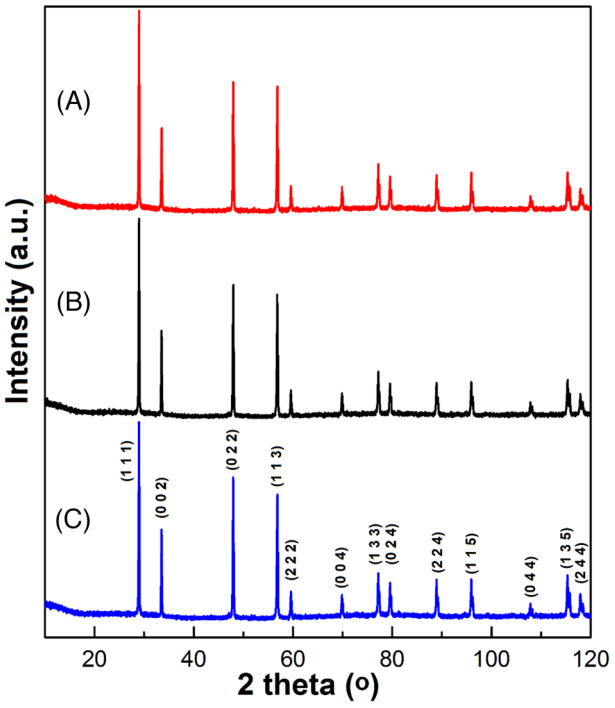

FIGURE 9 Effect of cooling rates: Eu6, 1°C/min (A); Eu5, 5°C/min (B), and Eu7, 10°C/min (C) showing $EuUO_4$ as the only crystalline phase

waste loadings and cooling rates, can provide good quality control on waste forms and guarantee that they meet the performance criteria. Note that slow cooling rates of ≤1°C/min are not practical as they can lead to undesirable large $LnUO_4$ crystals and glass crystallizations. This occurrence was observed in the sample prepared with a cooling rate of 1°C/min, with some $EuUO_4$ crystals growing larger than 10 μm (Figure S7). The backscattered SEM images (Figure 10) showed no obvious change in terms of gain sizes and characteristics of the ceramic crystallites. The stable microstructures again confirmed a reliable GC system that can provide a good quality assurance of the GC waste forms. Similar to the GC samples with variable waste loadings, the EDS analyses revealed an equal Eu:U atomic ratio in $EuUO_4$ crystallites with no obvious effect of cooling rate (at cooling rates above 5°C/min) on the Eu/U dissolution in residual glasses observed (Figure S7).

3.6 | Chemical durability

To further investigate the chemical durability of these $LnUO_4$–GC samples, Nd2 and Ho2 pellets with an equal ceramic-to-glass weight ratio (50 wt%:50 wt%) were made by mixing the oxide precursors with glass precursor and sintered at 1200°C for 6 h. The powder materials were prepared in accordance with the ASTM C1285 standard[55] and subjected to PCT leaching at 90°C for 7 days. The PCT leach results (Figure 11) showed low leach values for U and Nd/Dy (<0.05 g L^{-1}), consistent with their dominant presence in the durable $LnUO_4$ phases compared to

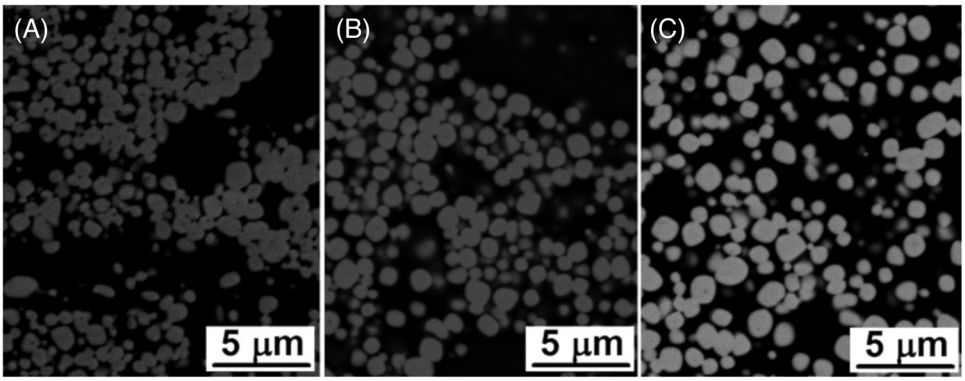

FIGURE 10 Backscattered scanning electron microscopy (SEM) images of Eu6, 1°C/min (A), Eu5, 5°C/min (B), and Eu7, 10°C/min (C) showing $EuUO_4$ as the only crystalline phase

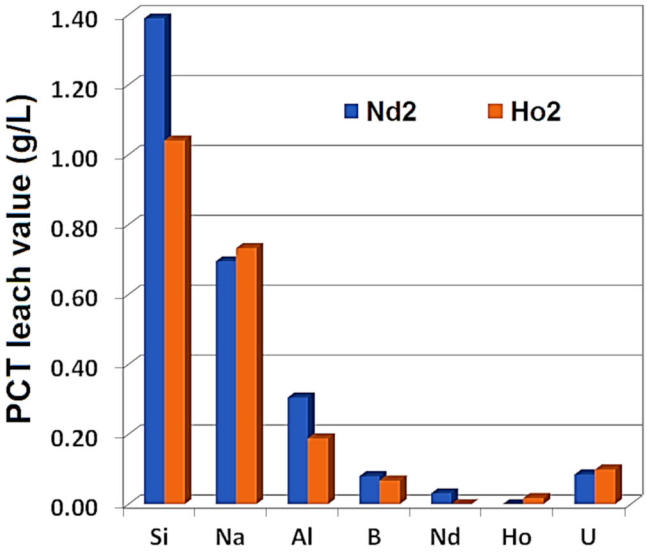

FIGURE 11 PCT leach values (g/L) for Nd2 and Ho2

their presence in residual glasses, which showed relatively higher leach values for Si (<1.4 g L^{-1}), Na (<0.8 g L^{-1}), and Al (<0.3 g L^{-1}). Overall, the designed $LnUO_4$–GC composite waste forms are chemically durable and suitable for the immobilization of the Ln–An fraction waste as well as other U-rich waste streams with substantial amounts of processing chemicals and impurities.

3.7 | Implications and perspectives

The similarity in the microstructures and XRD patterns in all $LnUO_4$–GC samples prepared by both processing routes (a pre-calcined $LnUO_4$ precursor and the in situ crystallization of $LnUO_4$ in glass from mixed oxides) confirmed the flexibility and versatility of the studied $LnUO_4$–GC system. The subtle microstructural change for the samples made at different waste loadings and cooling rates confirmed wide processing windows with regards to processing parameters. In addition, the in situ crystallization of $LnUO_4$ in glass was proved to be more reliable and suitable for waste form processing on an industrial scale.

The micro-cracking of GC composite waste forms from internal radiation damage must be taken into consideration. Most ceramic phases will become amorphous under internal α-decay damage with ~7 vol% swellings,[65,66] in contrast to the much lower swelling for borosilicate glasses. Consequently, the stress induced from the swelling of $LnUO_4$ crystallites in the residual glass may result in localized glass cracking, leading to increased leach rates. Such glass cracking can be minimized by reducing $LnUO_4$ crystallite sizes, allowing the relaxation of the residual glasses during swelling of the crystallites under alpha/gamma self-irradiation.[52] It is evident from current research that small $LnUO_4$ crystallites of sizes ranging between 1 and 5 μm can be formed in residual glasses with wide processing windows in terms of $LnUO_4$ waste loading and cooling rates (>1°C/min), suggesting a robust and promising GC composite system for future SNF management.

The success in making $LnUO_4$–GC composite waste forms by sintering in air has many implications in nuclear waste management. First of all, GC composite waste forms may provide a straightforward solution for the calcined Ln–An faction waste from the reprocessing of SNF. In addition, the high actinide waste loading of GC composites may provide a possible solution for SNF without reprocessing. The developed GC composite waste forms would also be suitable for the immobilization of many existing U-rich waste streams, such as DU waste from the U isotope enrichment for nuclear fuel production and the U-rich wastes from ^{99}Mo production, in the nuclear medicine sector.

Another implication to consider is candidate waste forms for the immobilization of minor actinides (Am^{3+} and Cm^{3+}). It is very challenging to immobilize minor

actinides (Am^{3+} and Cm^{3+}) with long half-lives in borosilicate glasses given the low solubility of their oxides in glasses.[46] The most acceptable way to address this issue is to incorporate such minor actinides in durable mineral phases such as zircon, zirconolite, pyrochlore, or phosphates.[30] Given their similar ionic radii (0.109 nm [Am^{3+}] and 0.097 nm [Cm^{3+}]; 0.1066 nm [Eu^{3+}], and 0.1017 nm [Ho^{3+}]), it is possible that $LnUO_4$–GC composite waste forms are suitable for immobilizing minor actinide ions. However, the speculation would require additional work and further validations.

Although $LnUO_4$–GC composites have demonstrated great potential as candidate waste forms for the immobilization of various U-rich waste streams, further studies are necessary to achieve more reliable and complete data to allow a detailed evaluation. The effect of sub-stoichiometry on crystalline phase formation and stabilization in glass should be investigated as Ln content is lower than U in many waste streams. In addition, pressure-assisted sintering methods, such as hot isostatic pressing, should be applied to produce dense $LnUO_4$–GC composite waste forms, allowing reliable evaluations of their chemical durability and the effect of radiation damage on chemical durability. As more accurate results become available through further research, the $LnUO_4$–GC composite materials will find practical applications in future nuclear waste management.

4 | CONCLUSIONS

The primary goal of this work was to investigate the feasibility of $LnUO_4$–GC composites as potential waste forms for the immobilization of the lanthanide fraction actinide waste from the reprocessing of SNF discharged from light water reactors. Consequently, $LnUO_4$–GC composites were successfully fabricated via two processing routes: the mixture of premade $LnUO_4$ crystalline precursor with glass precursor, followed by heat treatment; and in situ crystallization of $LnUO_4$ in glass from oxide precursors. The results indicated that both processing routes are quite robust with wide processing windows with regards to ceramic-to-glass ratios and cooling rates. In addition, PCT leaching results confirmed good chemical durability for the GC waste forms. Overall, $LnUO_4$–GC composite waste forms offer multiple processing options and the oxide route via direct sintering of mixed oxides is a reliable processing option for the immobilization of calcined lanthanide fraction actinide wastes after reprocessing of SNF. They will have implications for other U-rich waste streams such as DU wastes from U enrichment with substantial amounts of processing chemicals and impurities.

ACKNOWLEDGMENT

We would like to thank J. L. Abraham for his assistance with XRD data processing. All materials were synthesized and characterized at the facilities under Nuclear Science and Technology (NST), ANSTO. GLM is grateful to funding and support from the German Federal Ministry of Education and Research (BMBF), Project No. 02NUK060: Open access publishing facilitated by Australian Nuclear Science and Technology Organisation, as part of the Wiley – Australian Nuclear Science and Technology Organisation agreement via the Council of Australian University Librarians.

ORCID

Yingjie Zhang https://orcid.org/0000-0001-6321-4696

REFERENCES

1. Management of spent fuel from nuclear power reactors, learning from the past, enabling the future. Proceedings of an International Conference Held in Vienna, Austria, 24–28 June 2019. International Atomic Energy Agency; 2020.
2. zur Loye HC, Besmann T, Amoroso J, Brinkman K, Grandjean A, Henager CH, et al. Hierarchical materials as tailored nuclear waste forms: a perspective. Chem Mater. 2018;30:4475–88.
3. Ojovan MI, Lee WE. Glassy wasteforms for nuclear waste immobilization. Metall Mater Trans A. 2011;42(4):837–51.
4. Gregg DJ, Farzana R, Dayal P, Holmes R, Triani G. Synroc technology: perspectives and current status (review). J Am Ceram Soc. 2020;103(10):5424–41.
5. Lee WE, Gilbert M, Murphy ST, Grimes RW. Opportunities for advanced ceramics and composites in the nuclear sector. J Am Ceram Soc. 2013;96(7):2005–30.
6. Baker RJ. Uranium minerals and their relevance to long term storage of nuclear fuels. Coord Chem Rev. 2014;266–267:123–36.
7. Zhang Y, Lu KT, Zheng R. Synthetic uranium oxide hydrate materials: current advances and future perspectives. Dalton Trans. 2022;51:2158–69.
8. International Atomic Energy Agency. Status and trends in spent fuel and radioactive waste management. Vienna, Austria: IAEA; 2018.
9. Stefanovsky SV, Yudintsev SV, Shiryaev AA, Murzin VY, Trigub AL. Phase partitioning and uranium speciation in brannerite based ceramics. J Eur Ceram Soc. 2017;37:771–7.
10. Yudintsev SV, Stefanovsky SV, Nikol'skiia MS, Stefanovskaya OI, Nikonov BS. Brannerite, UTi_2O_6: crystal chemistry, synthesis, properties, and use for actinide waste immobilization. Radiochemical. 2016;58:333–48.
11. International Atomic Energy Agency (IAEA), Minimization of waste from uranium purification, enrichment and fuel fabrication, IAEA-TECDOC-1115, IAEA, 1999.
12. Farzana R, Zhang Y, Dayal P, Aly Z, Holmes R, Vance ER, et al. Pyrochlore glass-ceramics for the immobilization of uranium-bearing molybdenum-99 production wastes. J Eur Ceram Soc. 2021;41(14):7269–81.
13. Hertzler TJ, Nishimoto DD, Otis MD. Depleted uranium disposal options evaluation. Washington, DC, United States: USDOE; 1994. Web. https://doi.org/10.2172/10191353

14. Finch RJ, Ewing RC. The corrosion of uraninite under oxidizing conditions. J Nucl Mater. 1992;190:133–56.
15. Wronkiewicz DJ, Bates JK, Gerding TJ, Veleckis E, Tani BS. Uranium release and secondary phase formation during unsaturated testing of UO_2 at 90°C. J Nucl Mater. 1992;190:107–27.
16. Mesbah A, Szenknect S, Clavier N, Lin H, Baron F, Beaufort D, et al. Direct synthesis of pure brannerite UTi_2O_6. J Nucl Mater. 2019;515:401–6.
17. Bailey DJ, Stennett MC, Ravel B, Grolimund D, Hyatt NC. Synthesis and characterisation of brannerite compositions $(U_{0.9}Ce_{0.1})_{1-x}M_xTi_2O_6$ ($M = Gd^{3+}$, Ca^{2+}) for the immobilisation of MOX residues. RSC Adv. 2018;8:2092–9.
18. Zhang Y, Gregg DJ, Lumpkin GR, Begg BD, Jovanovic M. The incorporation of neptunium and plutonium in thorutite ($ThTi_2O_6$). J Alloys Compd. 2013;581:665–70.
19. Rossell HJ. Zirconolite—a fluorite-related superstructure. Nature, 1980;283:282–3.
20. Zhang Y, Stewart MSW, Li H, Carter ML, Vance ER, Moricca S. Zirconolite-rich titanate ceramics for immobilization of actinides – waste form/HIP can interactions and chemical durability. J Nucl Mater. 2009;395:69–74.
21. Vance ER, Lumpkin GR, Carter ML, Cassidy DJ, Ball CJ, Day RA, et al. Incorporation of uranium in zirconolite ($CaZrTi_2O_7$). J Am Ceram Soc. 2002;85(6):1853–9.
22. Xu H, Wang Y. Crystallization sequence and microstructure evolution of Synroc samples crystallized from $CaZrTi_2O_7$ melts. J Nucl Mater. 2000;279:100–6.
23. Vance ER, Ball CJ, Blackford MG, Cassidy DJ, Smith KL. Crystallisation of zirconolite from an alkoxide precursor. J Nucl Mater. 1990;175:58–66.
24. James M, Carter ML, Zhang Z, Zhang Y, Wallwork KS, Avdeev M, et al. Crystal chemistry and structures of (Ca,U) titanate pyrochlores. J Am Ceram Soc. 2010;93(10):3464–73.
25. Zhang Y, Li H, Moricca S. Pyrochlore-structured titanate ceramics for immobilization of actinides: hot isostatic pressing (HIPing) and stainless steel/waste form interactions. J Nucl Mater. 2008;377:470–5.
26. Gregg DJ, Zhang Y, Zhang Z, Karatchevtseva I, Blackford MG, Triani G, et al. Crystal chemistry and structures of uranium-doped gadolinium zirconates. J Nucl Mater. 2013;438:144–53.
27. Carter ML, Li H, Zhang Y, Vance ER, Mitchell DRG. Titanate ceramics for immobilization of uranium-rich radioactive wastes arising from ^{99}Mo production. J Nucl Mater. 2009;384:322–6.
28. Weber WJ, Wald JW, Matzke HJ. Effects of self-radiation damage in Cm-doped $Gd_2Ti_2O_7$ and $CaZrTi_2O_7$. J Nucl Mater. 1986;138:196–209.
29. Clavier N, Podor R, Dacheux N. Crystal chemistry of the monazite structure. J Eur Ceram Soc. 2011;31(6):941–76.
30. Dacheux N, Clavier N, Podor R. Monazite as a promising long-term radioactive waste matrix: benefits of high-structural flexibility and chemical durability. Am Miner. 2013;98:833–47.
31. Bregiroux D, Terra O, Audubert F, Dacheux N, Serin V, Podor R. Solid-state synthesis of monazite-type compounds containing tetravalent elements. Inorg Chem. 2007;46(24):10372–82.
32. Zhang Y, Vance ER. Plutonium in monazite and brabantite: diffuse reflectance spectroscopy study. J Nucl Mater. 2008;375:311–4.
33. Vance ER, Zhang Y, McLeod T, Davis J. Actinide valences in xenotime and monazite. J Nucl Mater. 2011;409:221–4.
34. Orlova AI, Orlova VA, Orlova MP, Bykov DM, Stefanovskii SV, Stefanovskaya OI, et al. The crystal-chemical principle in designing mineral-like phosphate ceramics for immobilization of radioactive waste. Radiochemical. 2006;48(4):330–9.
35. Orlova AI. Isomorphism in crystalline phosphates of the $NaZr_2(PO_4)_3$ structural type and radiochemical problems. Radiochemical. 2002;44(5):423–45.
36. Poojary DM, Clearfield A. Crystal structure of sodium zirconium phosphate, $Zr_2(NaPO_4)4.6H_2O$, from X-ray powder diffraction data. Inorg Chem. 1994;33(17):3685–8.
37. Strachan DM, Scheele RD, Buck EC, Icenhower JP, Kozelisky AE, Sell RL, et al. Radiation damage effects in candidate titanates for Pu disposition: pyrochlore. J Nucl Mater. 2005;345:109–35.
38. Murphy GL, Zhang Z, Tesch R, Kowalski PM, Avdeev M, Kuo EY, et al. Tilting and distortion in rutile-related mixed metal ternary uranium oxides: a structural, spectroscopic, and theoretical investigation. Inorg Chem. 2021;60:2246–60.
39. Cooper MWD, Gregg DJ, Zhang Y, Thorogood GJ, Lumpkin GR, Grimes RW, et al. Formation of $(Cr,Al)UO_4$ from doped UO_2 and its influence on partition of soluble fission products. J Nucl Mater. 2013;443:236–41.
40. Murphy GL, Kegler P, Zhang Y, Zhang Z, Alekseev EV, Daly de Jonge M, et al. High pressure synthesis, structural and spectroscopic studies of the Ni-U-O system. Inorg Chem. 2018;57(21):13847–58.
41. Miyake C, Isobe T, Yoneda Y, Imoto S. Magnetic properties of pentavalent uranium ternary oxides with fluorite structure: $ScUO_4$, YUO_4, CaU_2O_6 and CdU_2O_6. Inorg Chim Acta. 1987;140:137–40.
42. Popa K, Prieur D, Manara D, Naji M, Vigier JF, Martin PM, et al. Further insights into the chemistry of the Bi–U–O system. Dalton Trans. 2016;45:7847–55.
43. Weitzel H, Keller C. Neutron diffraction studies of $(RE_{0.5}U_{0.5})O_2$ (RE = Y, La, Nd, Ho, and Lu). J Solid State Chem. 1975;13:136–41.
44. de Alleluia IB, Hoshi M, Jocher WG, Keller C. Phase relationships for the ternary UO_2-UO_2-$REO_{1.5}$ (RE = Pr, Nd, Dy) systems. J Inorg Nucl Chem. 1981;43:1831–4.
45. Murphy GL, Zhang Z, Kennedy BJ. The solid-state chemistry of AUO_4 ternary uranium oxides: a review. In: Vogt T, Buttrey D, Editors. Complex oxides. Singapore: World Scientific; 2019.
46. Vance ER, Zhang Y, Gregg DJ. Ceramic waste forms. In: Konings R, Stoller R, editors. Comprehensive nuclear materials. 2nd Ed. Amsterdam. Elsevier; 2020.
47. Zhang Y, Zhang Z, Thorogood G, Vance ER. Pyrochlore based glass-ceramics for the immobilization of actinide-rich nuclear wastes: from concept to reality. J Nucl Mater. 2013;432(1–3):545–7.
48. Zhang Y, Gregg DJ, Kong L, Jovanovich M, Triani G. Zirconolite glass-ceramics for plutonium immobilization: the effects of processing redox conditions on charge compensation and durability. J Nucl Mater. 2017;490:238–41.
49. McCloy JS, Goel A. Glass-ceramics for nuclear-waste immobilization. MRS Bull. 2017;42(3):233–8.
50. Scales N, Dayal P, Aughterson RD, Zhang Y, Gregg DJ. Sodium zirconium phosphate based glass-ceramic composites as potential waste forms for the immobilization of nuclear wastes. J Am Ceram Soc. 2022;105:901–12.

51. Ojovan MI, Petrov VA, Yudintsev SV. Glass crystalline materials as advanced nuclear wasteforms. Sustainability. 2021;13:4117.
52. Zhang Y, Kong L, Ionescu M, Gregg DJ. Current advances on titanate glass-ceramic composite materials as waste forms for actinide immobilization: a technical review. J Eur Ceram Soc. 2022;42(5):1852–76.
53. Kong L, Karatchevtseva I, Zhang Y. A new method for production of glass–$Ln_2Ti_2O_7$ pyrochlore (Ln = Gd, Tb, Er, Yb). J Eur Ceram Soc. 2017;37(15):4963–72.
54. Kong L, Zhang Y, Karatchevtseva I. Preparation of $Y_2Ti_2O_7$ pyrochlore glass-ceramics as potential waste forms for actinides: the effects of processing conditions. J Nucl Mater. 2017;494:29–36.
55. ASTM C1285-21, Standard test methods for determining chemical durability of nuclear, hazardous, and mixed waste glasses and multiphase glass ceramics: the product consistency test (PCT), ASTM International, West Conshohocken PA, 2021.
56. Lu KT, Zhang Y, Wei T, Zhang Z, Avdeev M, Zheng R. An investigation of $LnUO_4$ (Ln = Dy and Ho): structures, microstructures, uranium valences and magnetic properties. J Eur Ceram Soc. 2021;41(12):6000–9.
57. Shannon RD. Revised effective ionic radii and systematic studies of interatomic distances in halides and chalcogenides. Acta Crystallogr Sect A: Cryst Phys Diffr Theory Gen Crystallogr. 1976;32:751–67.
58. Zhang Y, Karatchevtseva I, Kong L, Wei T, Zhang Z. Structural and spectroscopic investigations on the crystallization of uranium brannerite phases in glass. J Am Ceram Soc. 2018;101:5219–28.
59. Liu JH, van den Berghe S, Konstantinovic MJ. XPS spectra of the U5+ compounds KUO_3, $NaUO_3$ and $Ba_2U_2O_7$. J Solid State Chem. 2009;182(5):1105–8.
60. Finnie KS, Zhang Z, Vance ER, Carter ML. Examination of U valence states in the brannerite structure by near-infrared diffuse reflectance and X-ray photoelectron spectroscopies. J Nucl Mater. 2003;317:46–53.
61. Wilkins MCD, Mottram LM, Maddrell ER, Stennett MC, Corkhill CL, Kvashnina KO, et al. Synthesis, characterization, and crystal structure of dominant uranium(V) brannerites in the $UTi_{2-x}Al_xO_6$ system. Inorg Chem. 2022;60(23):18112–21.
62. Colella M, Zhang Z, Finnie KS, Smith KL, Buck EJ, Zhang Y. Determination of U-oxidation states in the brannerite structure by electron energy-loss (EELS), x-ray photoelectron (XPS) and diffuse reflectance (DRS) spectroscopies. Microsc Microanal. 2003;9:838–9.
63. Colella M, Lumpkin GR, Zhang Z, Buck EC, Smith KL. Determination of the uranium valence state in the brannerite structure using EELS, XPS, and EDX. Phys Chem Miner. 2005;32:52–64.
64. Zhang Y, Wei T, Zhang Z, Kong L, Dayal P, Gregg DJ. Uranium brannerite with Tb(III)/Dy(III) ions: phase formation, structures, and crystallizations in glass. J Am Ceram Soc. 2019;102(12):7699–709.
65. Lumpkin GR. Alpha-decay damage and aqueous durability of actinide host phases in natural systems. J Nucl Mater. 2001;289:136–66.
66. Lumpkin GR, Smith KL, Blackford MG. Heavy ion irradiation studies of columbite, brannerite, and pyrochlore structure types. J Nucl Mater. 2001;289:177–87.

SUPPORTING INFORMATION

Additional supporting information can be found online in the Supporting Information section at the end of this article.

How to cite this article: Lu KT, Zhang Y, Wei T, Murphy GL, Bhuiyan A, Scales N, et al. $LnUO_4$-based glass–ceramic composites as waste forms for the immobilization of lanthanide-bearing uranium wastes. J Am Ceram Soc. 2022;105:7697–7709. https://doi.org/10.1111/jace.18678